Poisson's ratio bounds in orthotropic materials. Application to natural composites: wood, bamboo and Arundo donax

Poisson's ratio bounds in orthotropic materials. Application to natural composites: wood, bamboo and *Arundo donax*

Lando Mentrasti [(1)], Luisa Molari [(2)], Marco Fabiani [(3)]

[(1)] DICEA, Università Politecnica delle Marche, Facoltà di Ingegneria, Via delle Brecce Bianche, Ancona, Italia, https://orcid.org/0000-0002-0915-3156

[(2)] DICAM, Alma Mater Studiorum - Università of Bologna, Viale Risorgimento 2, 40136, Bologna, Italia, https://orcid.org/0000-0001-6080-6194

[(3)] Scuola Secondaria, 61121, Pesaro, Italia, https://orcid.org/0000-0001-7370-1519

Abstract

The paper discusses the restrictions the positive definite character of the strain energy imposes to the values of the Poisson's ratios in a linear elastic orthotropic constitutive law. By exploiting the reciprocity principle and the conservation of energy, non-trivial constraints arise, leading to a particularly expressive form of the domain of existence, named *Tetrahedron-Ellipsoid* locus, in the space of three independent Poisson's ratios. The presented analysis establishes several notable restrictions for the elastic behavior of orthotropic composite materials, in all the cases in which there are great differences in the Young's moduli. For instance, near the *edge* of this locus, some Poisson ratios may belong to an interval not including the zero value; a very interesting peculiarity, perhaps not yet figured out in literature. In order to assess the coerciveness of the formulation, the results are applied to common wood essences, to several Italian growing species of bamboo and *Arundo donax*, natural composite functionally graded orthotropic materials. In the latter cases, an extensive experimental investigation is carried out to detect several Poisson's ratios, not studied in literature. Poisson ratios are obtained directly by strains measured by means of both physical strain gauges and Digital Image Correlation (DIC).

Keywords

Anisotropy, Mechanical properties, Wood, Analytical modelling, Mechanical testing.

1 INTRODUCTION

The anisotropic linear material is completely described by 21 constants at most, on which the thermodynamics imposes two kinds of restrictions: the Betti reciprocity and the positive definiteness of the strain energy. Unlike the isotropic material, whose unique Poisson's ratio is simply limited to the interval (-1, 0.5), for anisotropic behavior a full understanding of these restrictions is rather difficult to grasp.

While the first formulation of the restrictions in anisotropy have been stated by Voigt on 1910, a detailed modern discussion on the *orthotropic* behavior is given by Lempriere (1968) [1]. Later, Musgrave (1990) studies the constraints in general anisotropy, by factorizing the compliance matrix and also giving some graphical representation of the restrictions obtained [2].

The question of the *transversal* coupling in elastic behavior is particularly important within the scope of anisotropic composite materials. Milton (1995) discusses the realization of composites with *arbitrary* elastic parameters by combining two homogeneous material [3]. For cubic and hexagonal symmetries, Ting (2005) claims for the theoretical absence of limits of the Poisson's ratios, included negative values (auxetic) [4]. A microstructural justification of these cases, from a point of view of the solid-state physics, can be found in Greaves (2011) [5] and Tokmakova (2005) [6]. A brief history account of the Poisson's ratio identification can be found in Musgrave (1990), Greaves (2011) and Timoshenko (1953, Chap. VIII) [7].

The aim of this paper is, firstly, to give explicit form to the restrictions the Poisson's ratios have to satisfy in **orthotropic** elastic material; then, is to apply the presented formulation to naturally composite material like wood, bamboo and *Arundo donax*. The thermodynamic constraints, arranged in simplest way, result in an expressive geometrical 3D locus, named *Tetrahedron-Ellipsoid*, representing the **domain of existence** of three independent Poisson's ratios.

In applying this formulation to natural composites, the data available for several species of structural wood are checked for thermodynamic consistency. Whereas several Poisson's ratios are available in literature for wood [8-14], they are quantitatively and qualitatively rather scarce for bamboo [15-20] and *Arundo donax* [21]. Recently, one of the Poisson's ratios has been directly detected in bamboo compression tests [22]; besides, the strains thorough the wall of bending C-shaped specimens [23] is analyzed with the *Digital Image Correlation* technique [24].

Therefore, a number of experimental tests are carried out on bamboo and Arundo specimens, on purpose, to detect the Poisson's ratios also in transversal direction. The paper is organized as follows: Section 2 briefly summarizes the elastic problem; Section 3 derives the required restrictions, together with an appropriate 3D representation; Section 4 applies these constraints to the Poisson's ratios using the available values for wood and experimental data obtained for Italian growing bamboo and Arundo.

2 ORTHOTROPIC LINEAR ELASTICITY

The constitutive equations of a linearly elastic orthotropic material can be written separating the stress-strain response due to the normal and the shear components. In the

orthogonal system of coordinate $\{x_1, x_2, x_3\}$, *parallel to the orthotropic axes*, the Voigt notation of the compliance matrix is

$$\boldsymbol{\varepsilon} = \mathbf{D}\boldsymbol{\sigma} \tag{1}$$

$$\boldsymbol{\gamma} = \mathbf{G}^{-1}\boldsymbol{\tau} \tag{2}$$

being $\boldsymbol{\varepsilon} := [\varepsilon_1 \ \varepsilon_2 \ \varepsilon_3]^T$, $\boldsymbol{\sigma} := [\sigma_1 \ \sigma_2 \ \sigma_3]^T$, $\boldsymbol{\gamma} := [\gamma_{12} \ \gamma_{23} \ \gamma_{31}]^T$, $\boldsymbol{\tau} := [\tau_{12} \ \tau_{23} \ \tau_{31}]^T$,

$$\mathbf{D} := \begin{bmatrix} \frac{1}{E_1} & \frac{-\nu_{12}}{E_2} & \frac{-\nu_{13}}{E_3} \\ \frac{-\nu_{21}}{E_1} & \frac{1}{E_2} & \frac{-\nu_{23}}{E_3} \\ \frac{-\nu_{31}}{E_1} & \frac{-\nu_{32}}{E_2} & \frac{1}{E_3} \end{bmatrix} = \begin{bmatrix} 1 & -\nu_{12} & -\nu_{13} \\ -\nu_{21} & 1 & -\nu_{23} \\ -\nu_{31} & -\nu_{32} & 1 \end{bmatrix} \begin{bmatrix} \frac{1}{E_1} & & \\ & \frac{1}{E_2} & \\ & & \frac{1}{E_3} \end{bmatrix}, \tag{3}$$

and $\mathbf{G}^{-1} := diag[1/G_{12}, 1/G_{23}, 1/G_{31}]$ (obviously, $\gamma_{ij} = \gamma_{ji}$ and $\tau_{ij} = \tau_{ji}$).

The **Poisson's ratio** ν_{tn} is the ratio

$$\nu_{tn} := -\varepsilon_{\mathbf{t}} / \varepsilon_{\mathbf{n}}, \tag{4}$$

$\varepsilon_{\mathbf{n}}$ being the strain due to a *uniaxial* tension along a direction **n** and $\varepsilon_{\mathbf{t}}$ is the consequent strain in a direction $\mathbf{t} \perp \mathbf{n}$ (*indirect* effect).

The number of independent parameters necessary to identify an orthotropic material is twelve: *nine* elastic constants and *three* numbers locating the material symmetry triad, characterizing the orthotropy. Once the orthotropic axes are known, the independent parameters are the Young's moduli, E_i, the shear moduli, G_{ij}, and three Poisson's ratios, because the principle of conservation of energy imposes

$$\nu_{ij} / E_j = \nu_{ji} / E_i, \ i \neq j \tag{5}$$

Sometimes, the out of diagonal terms of the compliance matrix **D** are arranged in an alternative form: $D'_{ij} = \nu'_{ij}/E_i$. Obviously the relationships $\nu'_{ij}/E_i \equiv \nu_{ij}/E_j$ have to be true, so that the two versions are equivalent. However, the definition (4) explicitly

reveals the mechanical significance of ν_{ij} as the *indirect* strain effect of the uniaxial stress, both along the axes of orthotropy. On the contrary, using D'_{ij}, in the case of uniaxial traction along z, the Poisson's ratio ν_{yz} should be written in the misleading expression

$$\nu_{yz} := \frac{\nu'_{yz}}{E_y} \Big/ \frac{1}{E_z} = \nu'_{yz} \frac{E_z}{E_y}. \tag{6}$$

Note that Eq. (3) allows rapidly inverting the constitutive equation, as required for instance in FEM codes, as

$$\mathbf{D}^{-1} := \frac{1}{d} \begin{bmatrix} E_1 & & \\ & E_2 & \\ & & E_3 \end{bmatrix} \begin{bmatrix} 1-\nu_{23}\nu_{32} & \nu_{12}+\nu_{13}\nu_{32} & \nu_{13}+\nu_{12}\nu_{23} \\ \nu_{21}+\nu_{23}\nu_{31} & 1-\nu_{13}\nu_{31} & \nu_{23}+\nu_{21}\nu_{13} \\ \nu_{31}+\nu_{32}\nu_{21} & \nu_{32}+\nu_{31}\nu_{12} & 1-\nu_{12}\nu_{21} \end{bmatrix}, \tag{7}$$

where *d is*

$$d := 1-(\nu_{12}\,\nu_{21} + \nu_{23}\,\nu_{32} + \nu_{31}\,\nu_{13} + 2\,\nu_{12}\nu_{23}\nu_{31}). \tag{8}$$

3 POISSON RATIO'S CONSTRAINTS

3.1 Definite positiveness of the strain energy density

For the strain energy density to be positive, the matrices **D** and **G** must be positive definite, that is $\mathsf{G}_{ij} > 0$ and the eigenvalues of **D** have to be positive (§ 8.4.4) [25]. Since the eigenpairs of the compliance matrix is barely significant from a mechanical point of view, the last condition can be replaced by equivalent *strict* inequalities explicitly involving the engineering parameters E_i. The Sylvester's theorem and the multiplication theorem of determinant, gives the following equivalent conditions

$$\frac{1}{E_i} > 0,\ det\begin{bmatrix} 1 & -\nu_{ij} \\ -\nu_{ji} & 1 \end{bmatrix} > 0, det\begin{bmatrix} 1 & -\nu_{12} & -\nu_{13} \\ -\nu_{21} & 1 & -\nu_{23} \\ -\nu_{31} & -\nu_{32} & 1 \end{bmatrix} > 0. \tag{9}$$

Since the axes naming is immaterial, each relationship involving the elastic parameters generates further relationships, by a permutation of the axis indices.

The first condition leads to trivial relationships about the Young's moduli:

$$E_i > 0. \tag{10}$$

The second one gives

$$\nu_{ij}\,\nu_{ji} < 1,\ (i,j = 1, 2, 3). \tag{11}$$

The left hand side, using Eq. (5), is

$$\nu_{ij}\,\nu_{ji} = \nu_{ij}^2 \frac{E_i}{E_j} > 0. \tag{12}$$

Finally, Eqs. (11) becomes

$$\nu_{ij}^2 < \frac{E_j}{E_i}\,. \tag{13}$$

The last condition writes $d > 0$, namely

$$\nu_{12}\,\nu_{21} + \nu_{23}\,\nu_{32} + \nu_{31}\,\nu_{13} + 2\,\nu_{12}\nu_{23}\nu_{31} < 1, \tag{14}$$

using the identity

$$\nu_{21}\nu_{32}\,\nu_{13} \equiv \nu_{12}\nu_{23}\,\nu_{31}, \tag{15}$$

derived once again from Eqs. (5). It is interesting to notice that this relationship, unlike Eqs. (5), *does not involve the Young's moduli* and it is therefore rather useful in experimental investigations (together with the Eqs. (5)).

3.2 Relationships between reciprocal Poisson's ratio

By collecting Eqs. (11)-(13), a bilateral bound is obtained

$$0 < \nu_{ij}\,\nu_{ji} < 1. \tag{16}$$

First, since $0 < \nu_{ij}\,\nu_{ji}$ the *reciprocal* Poisson's ratios must have **the same sign**.

Second, $\nu_{ij}\,\nu_{ji} = |\nu_{ij}|\,|\nu_{ji}|$ and the inequality (16) can be rewritten in a more meaningful final form as

$$|\nu_{ij}| < \frac{1}{|\nu_{ji}|}\,, \tag{17}$$

namely:

the absolute value of a Poisson's ratio **may exceed unity** only if is its *reciprocal* absolute value **is less than 1**. Inversely, if the absolute value of a Poisson's ratio is *greater than unity*, then its reciprocal absolute value *must be less than 1*.

Expanding Eq. (13), the bilateral bounds for a single Poisson's ratio is related to the *associated* Young's moduli

$$-\sqrt{\frac{E_j}{E_i}} < \nu_{ij} < \sqrt{\frac{E_j}{E_i}}. \tag{18}$$

As a consequence:

two reciprocal Poisson's ratios may belong *both* to the range [1/2, 1);

by denoting with $E_{i_{MAX}}$ the maximal Young's modulus, then

$$\nu_{i_{MAX}j} < \sqrt{\frac{E_j}{E_{i_{MAX}}}} \leq 1\,, \tag{19}$$

that is, the Poisson's ratio **along** the direction of *maximum stiffness* **must be** *less than 1*.

Consequently, in the directions *orthogonal* to the *maximum stiffness* $\nu_{ji_{MAX}}$ **may** *exceed unity*.

3.3 The mixed constraint

First, the inequality (14), $\nu_{12}\nu_{23}\,\nu_{31} < (1 - \nu_{12}\nu_{21} - \nu_{23}\nu_{31} - \nu_{31}\nu_{13})/2$, can be majorized, in view of Eqs. (16) and (15), as

$$\nu_{12}\,\nu_{23}\,\nu_{31} = \nu_{21}\nu_{32}\nu_{13} < \frac{1}{2}\,. \tag{20}$$

The mechanical significance of inequality (14) is better investigate by:

first, rewriting it as a function of ν_{12}, ν_{23} and ν_{31} alone:

$$\nu_{12}^2\frac{E_1}{E_2} + \nu_{23}^2\frac{E_2}{E_3} + \nu_{31}^2\frac{E_3}{E_1} + 2\,\nu_{12}\nu_{23}\nu_{31} < 1; \tag{21}$$

then, introducing the positive ratios between the Young's moduli

$$\alpha_{ij}^2 := \frac{E_j}{E_i}, \tag{22}$$

which satisfy the obvious identity

$$\alpha_1\, \alpha_2\, \alpha_3 \equiv 1. \tag{23}$$

Then, the fundamental inequality becomes

$$\left(\frac{\nu_{12}}{\alpha_{12}}\right)^2 + \left(\frac{\nu_{23}}{\alpha_{23}}\right)^2 + \left(\frac{\nu_{31}}{\alpha_{31}}\right)^2 + 2\,\nu_{12}\nu_{23}\nu_{31} < 1. \tag{24}$$

These constraints define the domain of existence as the *interior* of a finite region of $\Re^3 \equiv\{\nu_{12},\nu_{23},\nu_{31}\}$ having a *simple* interpretation: a ***Tetrahedron-Ellipsoid.*** In fact, each cross-section of the locus with a plane orthogonal to a coordinate axis is an ellipse, whose principal axes are rotated proportionally to the product ($\nu_{12}\ \nu_{23}\ \nu_{31}$).

Furthermore, at the extremes, the ellipses degenerate into double straight lines, so that the (not differentiable) boundary has edges like to an inscribed tetrahedron.

The locus is *symmetric* with respect to the *axes* (but not with respect to the coordinate planes) and its algebraic form is *invariant* with respect to a *permutation* of the variables.

In order to simplify Eq. (24), even for the graphical representation, let consider the normalized variables

$$\xi_{ij} := \frac{\nu_{ij}}{\alpha_{ij}} = \nu_{ij}\sqrt{\frac{E_i}{E_j}}, \tag{25}$$

transforming Eq. (24) in the locus

$$\xi_{12}^2 + \xi_{23}^2 + \xi_{31}^2 + 2\,\xi_{12}\xi_{23}\xi_{31} < 1, \tag{26}$$

where identity (23) is taking into account.

Besides, Eqs. (11) can be now rewritten as

$$\xi_{ij}^2 < 1, \tag{27}$$

and Eq. (15), in the form

$$\xi_{12}\xi_{23}\xi_{31} < \frac{1}{2}\,. \tag{28}$$

The *Tetrahedron-Ellipsoid,* has several manifold components in $\Re^3$; however, due to the constraint (27) *within the cube* $\xi_{ij}^2 < 1$, the inequality (26), or (24), is the most restrictive condition.

Note that in all the relationships obtained, a permutation $ij \leftrightarrow ji$ is legitimate (maintaining the cyclic order) because of the coherence of the derivations, based on the reciprocity constraint (5).

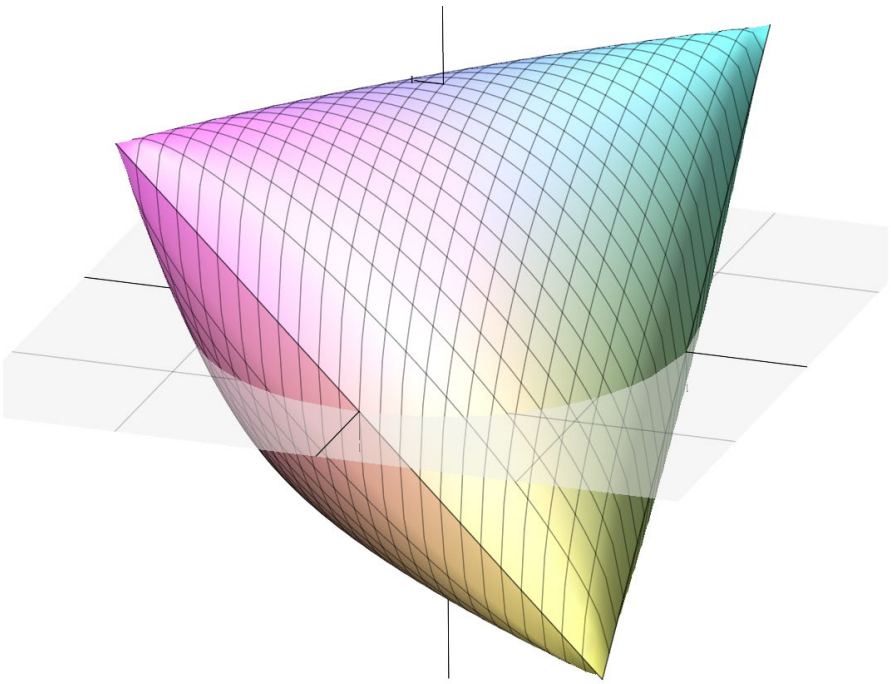

Fig. 1 – The *Tetrahedron-Ellipsoid*: the domain of existence of the three Poisson's ratios in normalized variables (notice the absence of the axis names, inessentials in this representation).

Fig. 1 shows the surface bounding this locus, in the normalized variables, where it can be recognize:

• the ellipses obtained cutting the locus with planes orthogonal to the coordinate axes, rotated by $\mp$ 45 degrees;

• the edges of the *tetrahedron* (double straight lines, degenerate conic);

• the circle at the intersection with the coordinate planes.

It is interesting to remark a notable consequence of this constrain, not identified in literature. Let $\mathfrak{E}$ be the ellipse obtained by a section of the locus, for instance, with a plane $\xi_{12} = a < 1$ and $a \approx 1$. Since the eccentricity of this ellipse is ≈ 1, the trace of a plane $\xi_{23} \approx 1$ does not intersect $\mathfrak{E}$ around the axis $\xi_{31} = 0$, as shown in Fig. 2. In explicit terms: the **range** of the admissible values of some ν_{ij} could **not contain zero**.

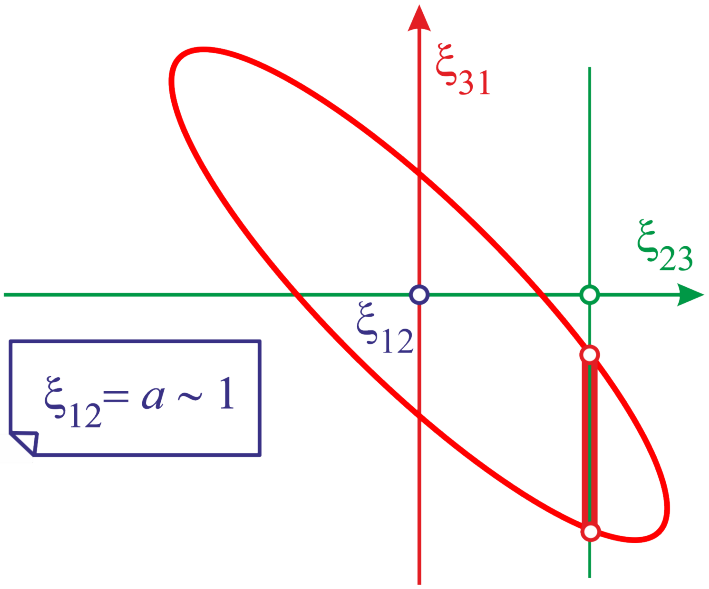

Fig. 2 – The range of ξ_{31} (namely ν_{31}) does not contain zero.

4 APPLICATION TO WOOD, BAMBOO AND ARUNDO DONAX

In the case of wood, as well as for bamboo or Arundo, the relationships are more readable if the orthotropy axes are referenced to radial, circumferential and longitudinal directions, $\{x_\rho, x_\varphi, x_z\}$, respectively (every indexed quantity being renamed, accordingly: *e.g.* $\alpha_{23} \rightarrow \alpha_{\varphi z}$).

It is important to emphasize that for such a kind of natural materials the numerical values of the mechanical characteristics have a greater intrinsic dispersion than for synthetic materials.

4.1 Application to Wood

The wood essences are studied rather extensively, so that a number of detailed experimental results are available in literature. The values of the Young's modulus and Poisson's ratios are derived from the Table 5-1 and 5-2 of the Wood Handbook (2010) at approximately 12% moisture content (notice that the original indexes are transposed).

Table 1 gives the ratios of the Young modulus and the Poisson's ratios, in the orthotropy directions, of several wood species. It can be noted that the ratios E_i/E_j can be rather far from unity and that the Poisson's ratios are often greater than 0.5. The last three columns show the percentage difference, $|\nu_{ij}/E_j - \nu_{ji}/E_i|$, with respect to the average value of that ratios, $(\nu_{ij}/E_j + \nu_{ji}/E_i)/2$: the reciprocity relationships (5) is verified for the great part of the cases with a deviation less than 10% (in green color). Only in few cases the error is greater than 33% (in red); although limited, this occurrence is not surprising considering the great variability of the source of the data collected in this table: for instance, the average Coefficient of Variation for the modulus of elasticity indicated by Wood Handbook, in Table 5-6, is 22 %.

Table 2 shows the values of the left hand of the inequalities the Poisson's ratios should satisfy (*cf.* the header of the first six column). The subsequent three columns test the equality (15), then the percentage difference is in the adjacent column. It is particularly reassuring that this stringent condition is verified by 10 species out 18 with an error less than 15% (green color), in consideration of the above reminded possible dispersion of the data due to different origin, ageing, test condition, *etc.*

Finally, the last column gives the value of the left hand of Eq. (14), largely less than one.

Species	E_φ/E_z	E_ρ/E_z	E_φ/E_ρ	$\nu_{\rho z}$	$\nu_{\varphi z}$	$\nu_{\varphi\rho}$	$\nu_{\rho\varphi}$	$\nu_{z\rho}$	$\nu_{z\varphi}$	Reciprocity ρz Δ%	Reciprocity φz Δ%	Reciprocity φρ Δ%
Hardwoods												
Ash, white	0,080	0,125	0,640	0,37	0,44	**0,68**	0,36	0,06	0,05	24,0	36,7	19,5
Aspen, quaking				0,49	0,37		0,50	0,05	0,02			
Balsa	0,015	0,046	0,326	0,23	0,49	**0,67**	0,23	0,02	0,01	52,3	20,6	**6,3**
Basswood	0,027	0,066	0,409	0,36	0,41	**0,91**	0,35	0,03	0,02	34,4	67,0	**7,5**
Birch, yellow	0,050	0,078	0,641	0,43	0,45	**0,70**	0,43	0,04	0,02	25,6	**6,2**	**4,8**
Cherry, black	0,086	0,197	0,437	0,39	0,43	**0,70**	0,28	0,09	0,05	10,8	26,4	**7,3**
Cottonwood, eastern	0,047	0,083	0,566	0,34	0,42	**0,88**	0,29	0,04	0,02	40,4	**9,2**	51,7
Mahogany, African	0,050	0,111	0,450	0,30	**0,64**	**0,60**	0,26	0,03	0,03	**0,1**	**0,2**	**3,0**
Mahogany, Honduras	0,064	0,107	0,598	0,31	**0,53**	**0,60**	0,33	0,03	0,03	**1,8**	**0,3**	**9,6**
Maple, sugar	0,065	0,132	0,492	0,42	0,48	**0,77**	0,35	0,07	0,04	14,9	17,8	**8,8**
Maple, red	0,067	0,140	0,479	0,43	**0,51**	**0,76**	0,35	0,06	0,04	**3,6**	25,3	**3,0**
Oak, red	0,082	0,154	0,532	0,35	0,45	**0,56**	0,29	0,06	0,03	17,1	10,7	**2,1**
Oak, white	0,072	0,163	0,442	0,37	0,43	**0,62**	0,30	0,07	0,04	20,7	15,5	**9,4**
Sweetgum	0,050	0,115	0,435	0,33	0,40	**0,68**	0,31	0,04	0,02	16,3	13,2	**4,1**
Walnut, black	0,056	0,106	0,528	0,50	**0,63**	**0,72**	0,37	0,05	0,04	**0,9**	**1,7**	**3,3**
Yellow-poplar	0,043	0,092	0,467	0,32	0,39	**0,70**	0,33	0,03	0,02	**2,5**	12,0	**0,1**
Softwoods												
Baldcypress	0,039	0,084	0,464	0,34	0,33	0,41	0,36					
Cedar, northern white	0,081	0,183	0,443	0,34	0,34	0,46	0,35					
Cedar, western red	0,055	0,081	0,679	0,38	0,30	0,48	0,40					
Douglas-fir	0,050	0,068	0,735	0,29	0,45	0,39	0,37	0,04	0,03		25,5	26,4
Fir, subalpine	0,039	0,102	0,382	0,34	0,33	0,44	0,34					
Hemlock, western	0,031	0,058	0,534	0,49	0,42	0,44	0,38					
Larch, western	0,065	0,079	0,823	0,36	0,28	0,39	0,35					
Pine												
Loblolly	0,078	0,113	0,690	0,33	0,29	0,38	0,36					
Lodgepole	0,068	0,102	0,667	0,32	0,35	0,47	0,38					
Longleaf	0,055	0,102	0,539	0,33	0,37	0,38	0,34					
Pond	0,041	0,071	0,577	0,28	0,36	0,39	0,32					
Ponderosa	0,083	0,122	0,680	0,34	0,40	0,43	0,36					
Red	0,044	0,088	0,500	0,35	0,32	0,41	0,31					
Slash	0,045	0,074	0,608	0,39	0,44	0,45	0,39					
Sugar	0,087	0,131	0,664	0,36	0,35	0,43	0,36					
Western white	0,038	0,078	0,487	0,33	0,34	0,41	0,33					
Redwood	0,089	0,087	1,023	0,36	0,35	0,37	0,40					
Spruce, Sitka	0,043	0,078	0,551	0,37	0,47	0,44	0,25	0,04	0,03	31,8	21,8	**2,1**
Spruce, Engelmann	0,059	0,128	0,461	0,42	0,46	**0,53**	0,26	0,08	0,06	42,3	72,1	**4,3**

Table 1 – Wood essences: literature data and reciprocity verification.

Species	$(\nu_{\varphi z})^2 E_\varphi/E_z < 1$	$(\nu_{\rho z})^2 E_\rho/E_z < 1$	$(\nu_{\varphi\rho})^2 E_\varphi/E_\rho < 1$	$\nu_{\rho z}\nu_{z\rho}$ **< 1**	$\nu_{z\varphi}\nu_{\varphi z}$ **< 1**	$\nu_{\varphi\rho}\nu_{\rho\varphi}$ **< 1**	$\nu_{\rho z}\nu_{z\varphi}\nu_{\varphi\rho} < 1/2$	$\nu_{z\rho}\nu_{\varphi z}\nu_{\rho\varphi} < 1/2$	Δ % Eq. (15)	*Locus* < 1
Hardwoods										
Ash, white	0,015	0,017	0,299	0,022	0,022	0,158	0,0129	0,0093	32	0,23
Aspen, quaking				0,026	0,008	0,186		0,0100		
Balsa	0,004	0,002	0,144	0,004	0,004	0,113	0,0014	0,0020	-39	0,12
Basswood	0,004	0,009	0,340	0,012	0,009	0,140	0,0073	0,0048	42	0,17
Birch, yellow	0,010	0,014	0,311	0,018	0,011	0,192	0,0071	0,0083	**-15**	0,24
Cherry, black	0,016	0,030	0,211	0,034	0,021	0,121	0,0131	0,0104	23	0,20
Cottonwood, eastern	0,008	0,010	0,434	0,015	0,008	0,123	0,0054	0,0053	**3**	0,16
Mahogany, African	0,021	0,010	0,164	0,010	0,021	0,169	0,0057	0,0056	**3**	0,21
Mahogany, Honduras	0,018	0,011	0,215	0,010	0,018	0,174	0,0064	0,0057	**11**	0,21
Maple, sugar	0,015	0,024	0,295	0,028	0,018	0,166	0,0121	0,0108	**12**	0,23
Maple, red	0,017	0,026	0,278	0,027	0,022	0,180	0,0146	0,0114	25	0,26
Oak, red	0,016	0,019	0,167	0,022	0,015	0,131	0,0065	0,0084	-26	0,18
Oak, white	0,013	0,022	0,169	0,027	0,015	0,128	0,0082	0,0095	**-15**	0,19
Sweetgum	0,008	0,012	0,202	0,014	0,009	0,125	0,0051	0,0055	**-7**	0,16
Walnut, black	0,022	0,026	0,272	0,026	0,023	0,232	0,0128	0,0121	**6**	0,31
Yellow-poplar	0,007	0,009	0,231	0,010	0,007	0,129	0,0042	0,0039	**9**	0,15
Softwoods										
Baldcypress	0,004	0,010	0,078			0,116				
Cedar, northern white	0,009	0,021	0,093			0,117				
Cedar, western red	0,005	0,012	0,159			0,119				
Douglas-fir	0,010	0,006	0,112	0,011	0,013	0,168	0,0033	0,0060	-59	0,20
Fir, subalpine	0,004	0,012	0,073			0,112				
Hemlock, western	0,006	0,014	0,104			0,162				
Larch, western	0,005	0,010	0,125			0,097				
Pine										
Loblolly	0,007	0,012	0,101			0,106				
Lodgepole	0,008	0,010	0,147			0,132				
Longleaf	0,007	0,011	0,080			0,125				
Pond	0,005	0,006	0,087			0,116				
Ponderosa	0,013	0,014	0,123			0,144				
Red	0,004	0,011	0,083			0,097				
Slash	0,009	0,011	0,122			0,172				
Sugar	0,011	0,017	0,122			0,125				
Western white	0,004	0,008	0,082			0,115				
Redwood	0,011	0,011	0,142			0,138				
Spruce, Sitka	0,009	0,011	0,104	0,015	0,012	0,114	0,0040	0,0046	**-12**	0,15
Spruce, Engelmann	0,013	0,023	0,129	0,035	0,027	0,118	0,0130	0,0098	28	0,20

Table 2 – Wood essences: constraints verification.

4.2 Application to Bamboo

4.2.1 Theoretical constraints

Since the bamboo culm has a greater degree of anisotropy than the wood, it is not useless to give a preliminary glimpse to the restrictions the theory predicts for the Poisson's ratios.

Median ratios for the Young's moduli can be estimated as follows (*cf.*Table 3 below)

$$\alpha^2_{\rho\varphi} \coloneqq \frac{E_\varphi}{E_\rho} \cong 1, \alpha^2_{\varphi z} \coloneqq \frac{E_z}{E_\varphi} \cong 20, \alpha^2_{z\rho} \coloneqq \frac{E_\rho}{E_z} \cong \frac{1}{20} \tag{29}$$

assuming

$E_z \approx 20$ GPa, for the *outer* side of the wall; the longitudinal modulus falls in a wide range of 12 ÷ 23 GPa, depending on the number of fibers for unit area [26] and it is, therefore, greatly variable with ρ;

$E_\varphi \approx E_\rho \approx 0.50$ GPa, being these moduli in the range 0.22 ÷0.50 GPa, [15].

With these values the domain of existence of $\nu_{\varphi z}$, as a function of $\nu_{\rho\varphi}$ and $\nu_{z\rho}$ is represented in Fig. 3.

When $\nu_{\varphi z} > 0$, the bounds (18), applied to *all* the Poisson's ratios, give

$$\begin{aligned} &\nu_{\rho\varphi} \lesssim 1 \quad \text{and } \nu_{\varphi\rho} \lesssim 1, \\ &\nu_{\varphi z} \lesssim 4.4 \quad \text{and } \nu_{z\varphi} \lesssim \mathbf{0.22}, \\ &\nu_{z\rho} \lesssim \mathbf{0.22} \quad \text{and } \nu_{\rho z} \lesssim 4.4, \end{aligned} \tag{30}$$

all satisfying automatically Eq. (17). The emphasized terms, serve as stringent controls to *falsify* the formulation.

For these values, the surface giving the *upper bound* of $\nu_{\varphi z}$, as a function of $\nu_{\rho\varphi}$ and $\nu_{z\rho}$, appears as in Fig. 3: *c)* and *d)* sketches two views of this locus cut at $\nu_{\varphi z} = 1$.

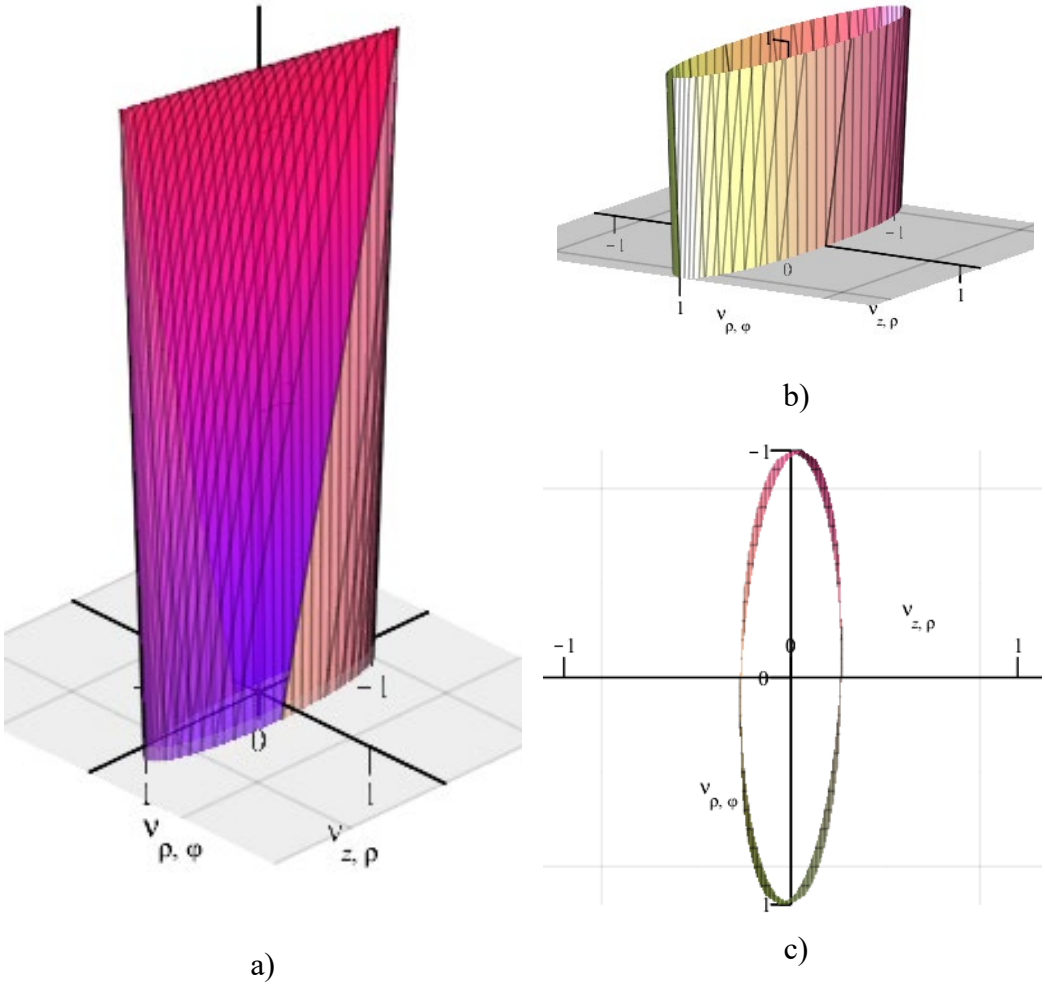

Fig. 3 – The *Tetrahedron-Ellipsoid* for a typical bamboo material (unscaled, positive values only), assuming $E_z / E_\varphi = 20$ and $E_\varphi \approx E_\rho$: *a)* and *b)* two views of $\nu_{\varphi z}$ as a function of $\nu_{\rho\varphi}$ and $\nu_{z\rho}$. In *b)* and *c)* the locus is cut at $\nu_{\varphi z} = 1.0$.

4.2.2 Experimental values

The data for bamboo elastic constants are not so easily available in particular for the transversal behavior (see *e.g.* Janssen, 1991 [27], Garcia, 2012 [15], Lee, 2014 [28], Moran, 2017 [29]). Table 3 reports a summary of some elastic parameters found in literature.

E_ρ	E_φ	E_z	$\frac{E_z}{E_\varphi}$	$\frac{E_\rho}{E_\varphi}$	$\nu_{\varphi z}$	$\nu_{\rho\varphi}$	$\nu_{\varphi\rho}$	Ref.
0.3 - 2.5	0.3 - 2.5	29.8 - 35.2	14.5	1		0.22	0.22	[28]
	0.53 - 0.49	21.13	40.1 - 42.9					[30]
	0.398		37.0			0.43 (B) 0.14 (M) 0.12 (T)		[15]
					0.32 (+)			[19]
					0.28 (+)			[18]
		14.59 (+) 12.58 (−)			0.26 (+) 0.34 (−)			[20]

(+) traction; (−) compression; Young's modulus in GPa.

Table 3 - Elastic characteristics of bamboo available in literature

All these experimental values widely satisfy the constraints indicated by the theory.

A recent extensive experimental investigation on five bamboo Italian growing species of *Phyllostachys bambusoides* (BAM)*, edulis* (EDU)*, iridescens* (IRI)*, vivax* (VIV)*, violascens* (VIO) is reported in [22]. In the compression tests, the Poisson's ratio $\nu_{\varphi z}$ is *directly* obtained by measuring the circumferential and longitudinal strain using physical strain-gauges (on the outer skin).

From these data, the Poisson's ratios are calculated in two different way: a macroscopic average and an incremental current value. The macroscopic *Average*-$\nu_{\varphi z}$ is defined as $\nu_{\varphi z} := -(\varepsilon_{\varphi,60} - \varepsilon_{\varphi,20})/(\varepsilon_{z,60} - \varepsilon_{z,20})$, following the indication of ISO 22157-1:2019 (subscripts denote the strains at 60% and 20% of the maximum test force, respectively).

As an alternative, an *Incremental*-$\nu_{\varphi z}$ is also computed as the ratio of the current increment of the strains, namely $\nu_{\varphi z} := -\Delta\varepsilon_\varphi / \Delta\varepsilon_z$, that is a function of the load, in general. This removes or mitigates several issues rising in the row experimental data, briefly discussed in Appendix. The relevant data are reported in Table 4, with the longitudinal Young's modulus, $E_{c,0}$, for sake of completeness.

Species	Number of samples	$E_{c,0}$	*Average*-$\nu_{\varphi z}$	*Incremental*-$\nu_{\varphi z}$
BAM	6	20.34	0.34	0.22 - 0.45
EDU	6	14.04	0.27	0.31 - 0.41
IRI	5	21.89	0.35	0.23 - 0.6
VIO	6	19.27	0.47	0.50 - 0.90
VIV	7	17.37	0.39	0.36 - 0.70

Table 4 - Poisson's $\nu_{\varphi z}$ ratio in compression test: physical strain-gauge.

Almost all tests show initial and final stages with an apparent pronounced nonlinearity or a susceptibility to the test rig adjustment. In any case, the central part of the pattern reveals that the current $\nu_{\varphi z}$, evaluated *incrementally*, is lightly smaller than the *averaged* one, with more or less dispersion (last column of Tab. 4 shows the extreme values). The species giving higher strength and modulus show also *great values of this Poisson's ratio*, up to about 0.5, apparently not previously detected in literature.

Fig. 4 shows some typical diagrams, with the aim to appreciate the quality of these kind of data.

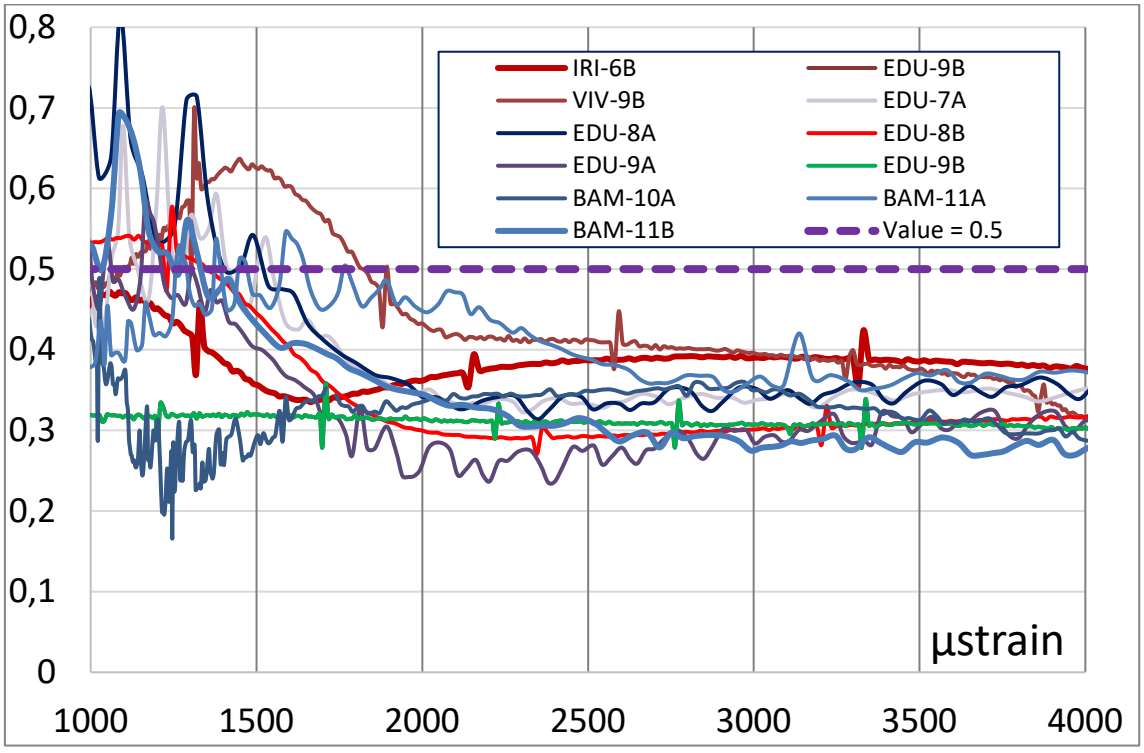

Fig. 4 – Typical diagrams of the Poisson's ratio in compression test (outer skin *physical* strain-gauge).

As an alternative, for three of these species, C-shaped specimens are subject to transversal bending using the so called ***C-shaped Bending tests*** [23]. In this test a thin *C-shaped* specimen is compressed diametrically. The ring is modelled as a thin arch so that the more stressed point, at the outer skin, is assumed to be in uniaxial state of stress. Then, the strains ε_ρ and ε_φ in this point of the annulus have measured by a virtual DIC strain gauge.

A subset of these species is tested employing the above-mentioned C-shaped specimens, under transversal bending (Fig. 5a): the circumferential and radial strains, near the outer skin of the cross-section, is measured by the DIC technique. The resulting $\nu_{z\varphi}$ are synthetized in Table 5, with the following meaning of the headers:

Linear, when the behavior is distinctly linear;

Nonlinear, when there is a clear deviation from linearity (at most quadratic) in at least one of the strains of the ratio (see Fig. 5);

Incremental ratio, when the computation of the incrementally computed Poisson's ratio is significantly different with respect to the coarse *Average* evaluation.

Species	Linear	Nonlinear	Incremental ratio
EDU2A	**0.30**		
EDU7A		0.33 - 0.47	0.5 - 0.55
EDU7B		0.38 - 0.42	0.48 - 0.2
EDU8A	**0.55**		
EDU8B	**0.54**		
EDU9B	**0.46**		
IRI1A	**0.55**		
IRI2B	0.41	0.65 - 0.42	0.51 - 0.29
IRI6A	**0.54**	0.65 - 0.51	
IRI6B	**0.65**	0.74 - 0.61	
VIO10A	**0.50**		
VIO9B	**0.54**	0.49 - 0.62	

Table 5 - Bamboo Poisson's ratio $\nu_{\varphi\rho}$ in *C-shaped* specimens (DIC virtual strain-gauge).

The boldface values indicate a very good linear behavior. In several cases, the response of the material shows a marked nonlinearity (the associated data are under the header *Nonlinear*). However, the differences with the values due to ta linear approximation, when computed, can be considered within the experimental tolerances (in red is reported the exception cases).

The examples sketched in Fig. 5 clearly show that the DIC technique have a much better accuracy than that obtained with the physical strain-gage. Therefore, the reliability of the data allows, on one hand, a faithful linear or quadratic interpolation smoothing; on the other hand, permits a correction of the zero, when occasionally this experimental error of indication is manifest, for one or both of the strain. The *Incremental ratio* automatically corrects this kind of error (*cf.* the discussion in Appendix).

Fig. 5 shows typical graphs: row data, interpolants, non- linearity, coarse Average ν and smoothed Poison's ratio.

Also, in these cases the values, reported in Table 4 and 5, satisfy the predicted constraints.

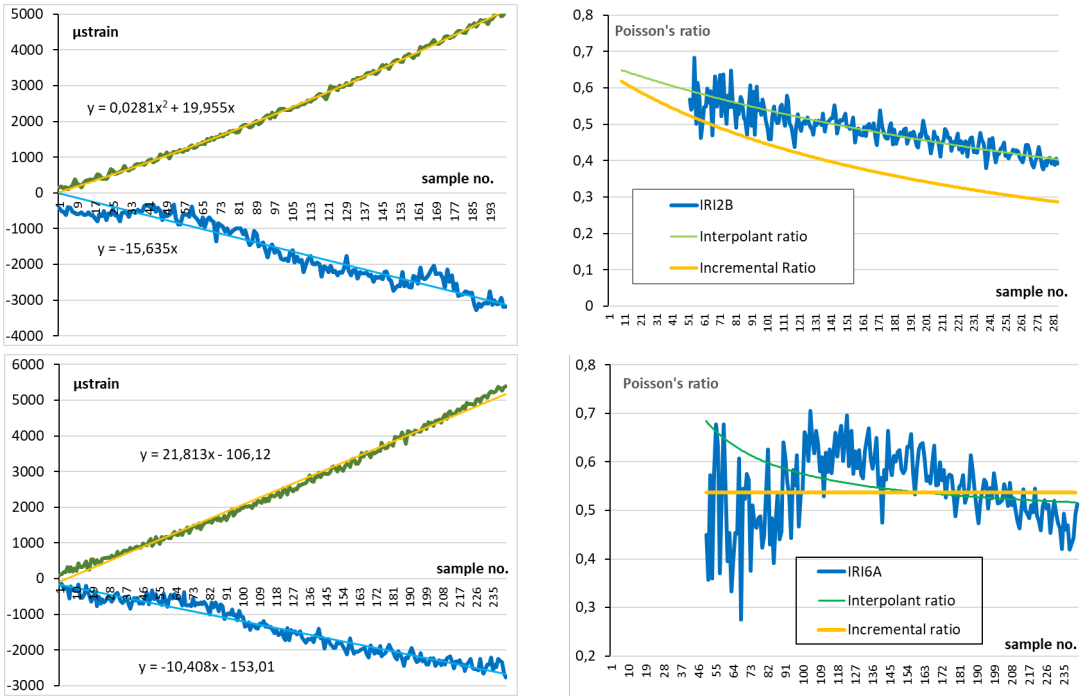

Fig. 5 – Bamboo Poisson's ratio $\nu_{\rho\varphi}$: typical data for *C-shaped* specimens using DIC virtual strain-gage. Interpolation curves (left): ε_φ (positive) and ε_ρ (negative), sample number in abscissa, IRI 2B, *(a)* and IRI 6A, *(c)*. Corresponding rough values of $\nu_{\rho\varphi}$, *Average*-$\nu_{\rho\varphi}$ and *Incremental*-$\nu_{\rho\varphi}$ Poisson's ratios in *(b)* and *(d)*.

4.3 Application to *Arundo donax*

Finally, a common *Arundo donax* reed is extensively investigated in compression, tension and employing the C-shaped bending test. In the last two cases, the strains are detected by DIC technique.

It is opportune to say in advance that, in these kinds of assays, the accuracy is much more critical than in the evaluation of a Young's modulus; furthermore, here it is strongly dependent on both the experimental technique and the species investigated. A large number of samples obtained from *Arundo donax* culms has been subject to Compression, Traction and *C-shaped* bending test. Table 6 shows these results, obtained with the DIC technique.

The great part of the *traction* cases shows an exemplary linear behavior.

Some *compressive* responses are partially irregular, mainly because of the influence of the friction on the very small Arundo specimens (height is equal to the diameter, 2-3 cm, according to the ISO 22157-1:2019).

Finally, the behavior of the specimens in the *C-shaped* bending test are almost all nonlinear, because of an evident deviation from linearity by at least one of the strain of the Poisson’s ratio. Some few extreme behaviors are in red.

In conclusion, also in these species the values of the Poisson’s ratios detected experimentally satisfy the above presented inequalities, almost trivially. Nonetheless, in several cases the crossing of the 0.5 threshold is unquestionable.

Species	Linear	Nonlinear	Incremental ratio
Compression			
pAD1A		0.61 - 0.38	0.73 - 0.05
pAD2A	0.70 - 0.61		
pAD3A		0.58 - 0.61	0.66 - 0.57
pAD1B		0.73 - 0.46	0.71 - 0.29
pAD2B		0.65 - 0.43	
pAD3B	0.58 - 0.61		
pAD1C		0.90 - 0.70	
pAD2C		0.86 - 0.78	
pAD3C		1.15 - 0.7	
Traction			
tAD1T	0.46		
tAD2T	0.45		
tAD3T	0.47		
tAD4T	0.49	0.52 - 0.49	
tAD6T	0.44		
tAD7T	0.44		
tAD8T	0.46		
C-Bending			
cAD1LC		0.48 - 0.39 - 0.42	0.32 - 0.44
cAD2LC		0.30 - 0.39	
cAD3LC		0.14 - 0.26	
cAD1MC		0.15 - 0.30	
cAD2MC		0.28 - 0.35	
cAD3MC		0.23 - 0.30	
cAD1NC		0.32 - 0.39	
cAD2NC	0.28		
cAD3NC	0.31 - 0.26		0.27
cAD10C		0.25 - 0.29 - 0.26	0.35 - 0.21
cAD20C		0.30 - 0.35	
cAD30C		0.33 - 0.36	

Table 6 - Poisson's $\nu_{\rho\varphi}$ ratio in Arundo specie (DIC virtual strain-gauge).

5 CONCLUSION AND FUTURE WORK

The principle of conservation of elastic strain energy in linear orthotropic material leads to several restrictions to the values the Poisson's ratios, ν_{ij}, may attain (beyond the almost trivial restrictions, $E_i > 0$, on the Yung moduli). The main constraints can be here summarized here:

$$\nu_{ij} / E_j = \nu_{ji} / E_i \,,$$

$\nu_{21}\nu_{32}\,\nu_{13} \equiv \nu_{12}\nu_{23}\,\nu_{31}$

$\nu_{ij}^2 < \frac{E_j}{E_i}$,

$\nu_{i_{MAX}j} < \sqrt{\frac{E_j}{E_{i_{MAX}}}} \leq 1$.

$\xi_{12}^2 + \xi_{23}^2 + \xi_{31}^2 + 2\,\xi_{12}\xi_{23}\xi_{31} < 1$

in *normalized* variables $\xi_{ij} := \frac{\nu_{ij}}{\alpha_{ij}} = \nu_{ij}\sqrt{\frac{E_i}{E_j}}$.

These inequalities describe a *Tetrahedron-Ellipsoid* surface. The inspection of this locus, near the *edge of the tetrahedron,* shows that some ν_{ij} may belong to an interval not including the zero value: a very interesting peculiarity, perhaps hitherto not recognized at all.

The obtained formulation is then applied to natural composite functionally graded orthotropic materials, like wood, bamboo and Arundo. The values of the elastic parameters, E_i and ν_{ij}, of the common **orthotropic wood** essences largely satisfy the restrictions.

For the **bamboo**, assuming average Young's moduli: $E_\varphi \approx E_\rho$, $E_z \approx 20\,E_\varphi$, the constraints read:

$\boldsymbol{\nu_{\rho\varphi} \lesssim 1}$ and $\nu_{\varphi\rho} \lesssim 1$

$\nu_{\varphi z} \lesssim 4.4$ and $\boldsymbol{\nu_{z\varphi} \lesssim 0.22}$

$\boldsymbol{\nu_{z\rho} \lesssim 0.22}$ and $\nu_{\rho z} \lesssim 4.4$,

becoming more and more stringent with increasing the disproportion between the Young moduli.

Several Italian growing species of bamboo and *Arundo donax* reeds are tested in compression, traction and using a special designed *C-shaped* specimen. Both in the

wood and in these species, the values of the Poisson's ratios detected experimentally satisfy the above presented inequalities. Nonetheless, the 0.5 threshold of the Poisson's ration is unquestionably traversed.

According to the above discussion, the more different are the Young's moduli greater are the restrictions on some of the Poisson's ratios. In this regard, it is decisive the detection of the longitudinal-circumferential coupling in bamboo culms. It requires an accurate design of a targeted test, a challenging objective in view of the small dimension of the sample, the difficult involved in the loading transfer and in the possible noise in the results obtained.

Appendix A. Issues on Poisson's measure: correction of row data

The strain data, along two orthogonal directions, are typically affected by a not negligible noise, as shown in Fig. A.1: part of it having a random character, part caused by a possible systematic error.

Therefore, a *direct* computation of the Poisson's ratio leads to the *zigzag* graph shown in Fig. A.2(a), because of several con-causes: the somewhat significant absolute error on each operand of the ratio; the relatively small value of it; the random character of the algebraic sign of the errors during the test. The consequence is an almost inacceptable amplification of the noise contained in each signal, leading a result almost unintelligible.

The direct use of the definition of the Poisson's ratio, Eq. (4), is operationally unfeasible, because of:

(*i*) the *error of the zero* of the transducer's indicators (force, displacement, strain, etc.); due to slipping and grip-rig adjustments of the specimen or to an error in the virtual strain gauge initial calibration (DIC).

(*ii*) some degree of *material nonlinearity*: it can appear in several phases of the test due to intrinsic nonlinear behavior or to the non-homogeneous load distribution in the specimen (that is naturally highly functionally graded), with special reference to the compression tests;

(*iii*) initial adjustments of the test-rig.

The idea is to regularize the data, by using their interpolant instead of the row values: linear, when possible, or at most quadratic fitting. A similar procedure is suggested by the norm ASTM E132-17, § 8.

The choice of the interpolant is firstly carried out without constrains. However, in case the obtained *residual strain* at the zero abscissa is not negligible, then a shift of the ordinate (or, rarely, also of the abscissa) corrects the baseline. Sometime, as a simple alternative, an interpolation with constraint to pass through the origin is employed. Finally, it should be remark that in case of *intrinsic nonlinearity* (of at least one of the terms) the ratio between the *total* strains has no sense from the linear elastic behavior point of view. On the contrary, it remains valid to consider the ratio between the **increment** of the strains between two consecutive steps of the load: $\nu_{ij}(\text{load}) := -\Delta\varepsilon_i / \Delta\varepsilon_j$, by interpreting it as a *tangent modulus.* Furthermore, the variation of this tangent Poisson's modulus through the test, and its comparison with the *average* Poisson's ratio, assumes the meaning of an indirect measure of the quality of the response.

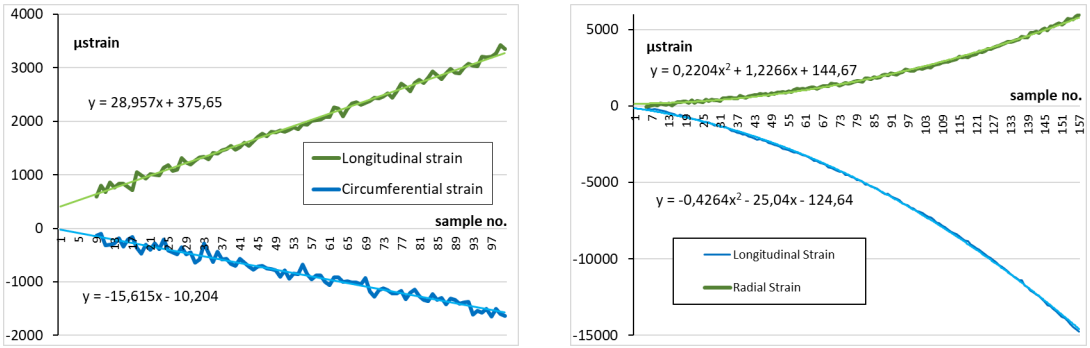

(a) *(b)*

Fig. A.1 – Row strains data: *(a)* a sharp linear behavior with a marked error of the zero indication [EDU-8B compression]; *(b)* evident nonlinear behavior with increasing loading [Arundo C-specimen C_AD2LC].

The result of this operation is synthetically showed in Fig. A.2:

- in abscissa, there are the ordinal number of the uniformly sampled signal (Fig. A.1 and A.2*b)*. It is linearly dependent on the global displacement, monotonically increasing during the test (carried out on a Universal Testing Machine under displacement control);

- the oscillations of the Poisson's ratio are now correctly ordered (coherent with the ratio of the interpolants) (the opposite case is in Fig. A.2 *a*);

- the correction of the error of the zero, may leads to a significant adjustment of the response (Fig. A.2 *b*).

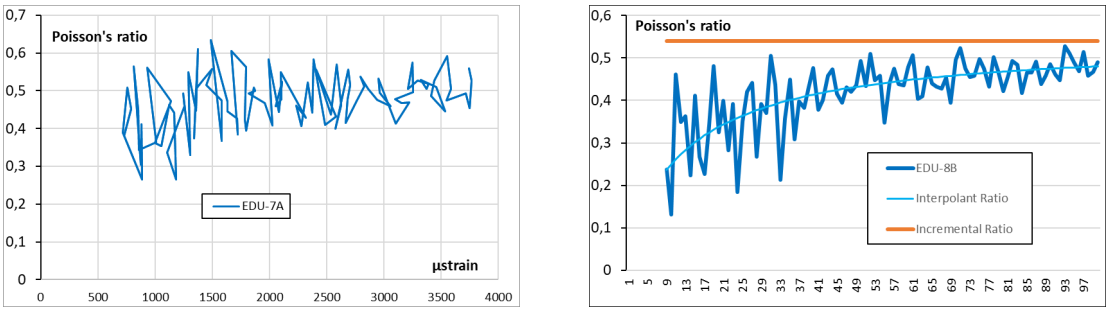

(a) *(b)*

Fig. A.2 – (a) "Chaotic" Poisson's ratio as a consequence of the ratio of non-smoothed values of the experimental strains [EDU-7A]; (b) Regularized patters: *ordering* with the total displacement; ratio of the interpolated values; incremental ratio (with correction of the zero error) (EDU-8B compression, *cf.* Fig. A.1 a).

A final experimental note: computing the *Incremental* Poisson's ratio with the divided differences on *three* points give no substantial improvement of the results, whilst a more sophisticated data smoothing technique appears to be incongruous in this intrinsically noised problem.

References

[1] Lempriere BM. Poisson's Ratio in Orthotropic Materials. AIAA Journal (1968) 2226-2227.

[2] Musgrave MJP. On the constraints of positive-definite strain energy in anisotropic elastic media. Quarterly Journal of Mechanics and Applied Mathematics **43**(4) (1990) 605-621.

[3] Milton GW, Cherkaev AV. Which Elasticity Tensors are Realizable? Journal of Engineering Materials and Technology **117**(4) (1995) 483-493.

[4] Ting TC, Barnett DM. Negative Poisson's Ratios in Anisotropic Linear Elastic Media. Journal of Applied Mechanics **72**(6) (2005) 929-931.

[5] Greaves GN, Greer AL, Lakes RS, Rouxel T. Poisson's ratio and modern materials. Nature Materials **10**(2011) 823-837.

[6] Tokmakova SP. Stereographic projections of Poisson's ratio in auxetic crystals. Physica Status Solidi (b) **242**(3) (2005) 721–729.

[7] Timoshenko STP. History of the Strength of Materials. McGraw-Hill (1953), Dover (1983)

[8] Jeong GY, Hindman DP, Zink-Sharp A. Orthotropic properties of loblolly pine (Pinus taeda) strands. Journal of Material Science **45**(2010) 5820–5830.

[9] Mascia NT, Nicolas EA. Determination of Poisson's ratios in relation to fiber angle of a tropical wood species. Construction and Building Materials **41**(2013) 691-696.

[10] Kohlhauser C, Hellmich C. Determination of Poisson's ratios in isotropic, transversely isotropic, and orthotropic materials by means of combined ultrasonic-mechanical testing of normal stiffnesses: Application to metals and wood. European Journal of Mechanics - A/Solids **33**(2012) 82-98.

[11] Moya L, Laguarda MF, Cagno M, Cardoso A, Gatto F, O'Neill H. Physical and Mechanical Properties of Loblolly and Slash Pine Wood from Uruguayan Plantations. Forest Products journal **63**(3/4) (2013) 128-137.

[12] Gibson LJ. The hierarchical structure and mechanics of plant materials. J. R. Soc. Interface **9**(2012) 2749-2766.

[13] Kumpenza C, Matz P, Halbauer P, Grabner M, Steiner G, Feist F, Müller U. Measuring Poisson's ratio: mechanical characterization of spruce wood by means of non-contact optical gauging techniques. Wood Science and Technology **52**(2018) 1451–1471.

[14] *Wood handbook. Wood as an engineering material*. General Technical Report FPL-GTR-190. Forest Products Laboratory, Department of Agriculture (2010) Madison, WI.

[15] García JJ, Rangel C, Ghavami K. Experiments with rings to determine the anisotropic elastic constants of bamboo. Construction and Building Materials **31**(2012) 52-57.

[16] Krause JQ, de Andrade Silva F, Ghavami K, da Fonseca Martins Gomes O, Dias Toledo Filho R. On the influence of Dendrocalamus giganteus bamboo

microstructure on its mechanical behavior. Construction and Building Materials **127**(2016) 199–209.

[17] Wang YZ, Zhang CL, Chen WQ. An analytical model to predict material gradient and anisotropy in bamboo. Acta Mechanica **228**(2017) 2819–2833.

[18] Aiping Z, Dongsheng H, Haitao L, Yi S. Hybrid approach to determine the mechanical properties of fibers and matrixes of bamboo. Construction and Building Material **35**(2012) 191-196.

[19] Cox FB, Geymayer HG. Expedient reinforcement for concrete for use in southeast asia, Report I. US Army Engineer Waterways Experiment Station Technical Report C-69-3 (1969) Vicksbury, Mississipi.

[20] Ghavami K, Marinho AB. Propriedades fisicas e mecanicas do colmo inteiro do bambu da espécie Guadua angustifolia. Revista Brasileira de Engenharia Agricola e Ambiental. **9**(1) (2005) 107:114.

[21] Molari L, Coppolino F., Garcia JJ. *Arundo donax*: a widespread structural material with great potential, *submitted*.

[22] Molari L, Mentrasti L, Fabiani, M. Mechanical characterization of five species of Italian bamboo. Structures **24**(2020) 59-72.

[23] Molari L, Garcia JJ. On the radial variation of the transverse mechanical properties of bamboo. Journal of Building Engineering **33**(2021).

[24] Zhao J, Sang Y, Duan F. The state of the art of two-dimensional digital image correlation computational method. Engineering Reports **1**(2) (2019) 1-15.

[25] Rees DWA. Mechanics of elastic solids. (2019) World Scientific Publishing.

[26] Janssen JJA. *Designing and Building with Bamboo*. International Network for Bamboo and Rattan (2000).

[27] Janssen JJA. *Mechanical properties of bamboo*. Kluwer Academic Publishers (1991).

[28] Lee PH, Odlin M, Yin H. Development of a hollow cylinder test for the elastic modulus distribution and the ultimate strength of bamboo. Construction and Building Materials **51**(2014) 235–243.

[29] Moran R, Webb K, Harries KA, García JJ. Edge bearing tests to assess the influence of radial gradation on the transverse behavior of bamboo. Construction and Building Materials **131**(2017) 574–584.

[30] Sharma B, Harries KA, Ghavami K. Methods of determining transverse mechanical properties of full-culm bamboo. Construction and Building Materials **38**(2013) 627–637.

[31] ISO 22157:2019 Bamboo structures — Determination of physical and mechanical properties of bamboo culms — Test methods.

[32] ASTM E132-17 Standard Test Method for Poisson's Ratio at Room Temperature.

Nomenclature

$\alpha_{ij}^2 \coloneqq \frac{E_j}{E_i}$

$\nu_{tn} \coloneqq \varepsilon_{\mathbf{t}} / \varepsilon_{\mathbf{n}}$ Poisson's ratio, normal strain in direction **t** due to a *uniaxial* state of stress along **n**;

$\boldsymbol{\varepsilon}, \boldsymbol{\gamma}, \boldsymbol{\sigma}, \boldsymbol{\tau}$ normal and shear component of the strain and stress tensor, respectively (in the Voigt form);

$\xi_{ij} \coloneqq \frac{\nu_{ij}}{\alpha_{ij}} = \nu_{ij}\sqrt{\frac{E_i}{E_j}}$

D compliance matrix of the normal components

E_i, G_{ij} Young's and shear moduli, respectively

$\{x_1,x_2,x_3\}$ system of orthogonal coordinate, along the axes of orthotropic symmetry.